

Using PySiUltraLight to Model Scalar Dark Matter with Self-Interactions

Noah Glennon* and Chanda Prescod-Weinstein†

Department of Physics and Astronomy, University of New Hampshire, Durham, New Hampshire

We introduce PYSiULTRALIGHT, a modification of the PYULTRALIGHT code that includes self-interaction terms to model the dynamical evolution of axion fields. PYULTRALIGHT simulates ultralight dark matter dynamics. We will use a boson mass of $10^{-22}\text{eV}/c^2$ in this paper. We use PYSiULTRALIGHT to produce collapsing solitons, spatially oscillating solitons, and exploding solitons which prior analytic work shows will occur with attractive self-interactions. We test the maximum mass criteria described in [1] for a soliton to collapse when attractive self-interactions are included. Implementing an approximate Gaussian ansatz for the wave function of the solitons, we calculate the oscillation frequency as a function of soliton mass and equilibrium radius in the presence of attractive self-interactions. We verify our code and that when the soliton mass is below the critical mass ($M_c = \frac{\sqrt{3}}{2}M_{\text{max}}$) described in [1] and the initial radius is within a specific range, solitons are unstable and explode. We also analyze both binary soliton collisions and a soliton rotating around a central mass with attractive and repulsive self-interactions. We find that when attractive self-interactions are included, the density profiles get distorted after a binary collision. We also find that a soliton is less susceptible to tidal stripping when attractive self-interactions are included. We find that the opposite is true for repulsive self-interactions in that solitons would be more easily tidally stripped.

I. INTRODUCTION

There is significant evidence to show that dark matter makes up the majority of the matter in the universe and that this dark matter is non-relativistic and collisionless [2–5]. Strong evidence for this cold dark matter (CDM) picture comes from fluctuations in the cosmic microwave background [6, 7]. We still know very little about the microphysics of the particle or particles that comprise dark matter. One of the most successful and well-studied dark matter paradigms is weakly-interacting massive particles (WIMPs). WIMPs are consistent with many of the large scale structures formed in the universe, but, at small scales, questions remain. Models, such as the WIMP model and other cold, collisionless models, with only dark matter predict dense cusps at the center of dark matter halos, but dark matter halos have constant density cores in observations and other simulations. This apparent issue may be resolved with the inclusion of baryonic processes such as supernova feedback, tidal stripping, and dynamical friction [8, 9]. Traditional CDM models like WIMPs also face the missing satellite problem, which refers to the discrepancy between the few subhalos we observe and the number found in CDM simulations. There are several proposed theoretical solutions to problem [2, 10–12]. This problem might also be fixed as physicists are finding more subhalos. WIMPs also face the “too big to fail” problem, which comes from the most dense dwarf galaxy-hosting subhalos being systematically denser than what we infer from the brightest Milky Way satellite galaxies [13]. This problem might also be solved by including baryonic effects such as supernova feedback and tidal stripping [8, 9].

Although these issues could be explained through the inclusion of baryonic processes, another possible solution is that a different dark matter model than WIMPs is needed. Axion-like particles (ALPs), which are motivated by open problems in QCD and also can come from string theory compactifications, are one such alternative dark matter candidate [2, 4, 14, 15]. This class of scalar dark matter particles has its roots in the QCD axion, which is a consequence of the Peccei-Quinn mechanism that was developed to solve the CP problem in QCD. The axion arises in this model through spontaneous symmetry breaking as a pseudo-Nambu-Goldstone boson [16]. The QCD axion potential is given by:

$$V(\phi) = \Lambda^4 (1 - \cos(\phi/f_a)) \quad (1)$$

where f_a is the CP symmetry breaking scale and $\Lambda \approx 0.1\text{GeV}$ [17]. Axion dark matter models can give close to the expected dark matter abundance we see in the universe [18–21]. From [17], the abundance of QCD axion dark matter is given by:

$$\Omega_a \approx \left(\frac{f_a}{10^{11-12}\text{GeV}} \right)^{7/6}. \quad (2)$$

The QCD axion is typically theorized to be more massive than the ALPs that are motivated by string compactifications. The mass of the QCD axion has a range of values but is estimated to be between $10 - 10^3 \mu\text{eV}$ [22]. These stringy ALPs are also sometimes referred to as ultralight axions (ULAs). Fuzzy dark matter (FDM) is a ULA model where dark matter comprises ultralight bosons $\sim \mathcal{O}(10^{-22})\text{eV}/c^2$ [23–25]. Because the mass of fuzzy dark matter is very small, the de Broglie wavelength is large (on the order of a kiloparsec) which means that dense cusps would be suppressed by quantum pressure. Here, quantum pressure is a term used to describe the effective particle-particle interaction that is found in

* nglennon@wildcats.unh.edu

† chanda.prescod-weinstein@unh.edu

the Madelung formalism [26]. Due to the wave-like nature of ULA models, on small scales, we should observe interference patterns [4, 27, 28]. ULA models have similar predictions to WIMP models on large scales. However, on small scales, ULA models have dark matter halos that will not form on scales smaller than the Jeans scale [23, 29]. Focusing on small-scale structures is therefore important in determining the nature of dark matter. Notably, this focus on ULAs leads to distinct phenomenological considerations from those with more massive ALPs, which can lead to miniclusters of cosmological interest, see e.g., [30, 31].

Typically ULA models, and more generally scalar dark matter models, ignore self-interactions between the particles in favor of considering only their coupling through gravity. ULA models that include self-interactions may diverge from those that are gravity-only [1]. If the self-interaction is attractive, as is the case with the QCD axion, virialized dark matter clusters of sufficient mass may collapse into black holes, explode, or oscillate in size. Supermassive black holes could be formed by ultralight particles such as ALPs with an attractive self-interaction. Meanwhile, the presence of a repulsive self-interaction guarantees the existence of a stable halo configuration [1]. This configuration occurs when the repulsive self-interaction and repulsive quantum pressure balance gravity's attractive behavior. In the scenario where the scalar dark matter has a repulsive self-interaction, observations from the Bullet Cluster set a limit on the scalar dark matter mass to be on the order of $m = 10^{-2} \text{eV}/c^2$ which is far too massive to be considered an ultralight axion [32].

To better quantitatively understand the effects of self-interactions on ULA models, we introduce PYSIULTRALIGHT, a modified version of PYULTRALIGHT which simulates the dynamics of axion fields [33], which solves the Schrödinger-Poisson equations. Our code modifies the original by including self-interactions. We validate the code by verifying the analytic predictions made in [1]. In particular, we confirm the existence of a maximum soliton mass, the oscillation behavior of solitons, and the conditions under which exploding solitons will occur given attractive self-interactions. We also explore the behavior of solitons in binary collisions and in orbits around a central potential when there are attractive self-interactions.

The contents of the paper are as follows. Section II outlines the physics of ULA models with the inclusion of self-interactions and describe the Gross-Pitaevskii-Poisson equations in dimensional and adimensional forms. Section III show how the equations of motion are implemented in PYSIULTRALIGHT. In Section IV, we discuss results found with PYSIULTRALIGHT, including analysis for finding the maximum mass for a soliton with attractive self-interactions, finding the oscillation frequencies of a soliton with attractive self-interactions, testing the conditions under which exploding solitons can occur. In Section V, we discuss simulations of both binary soliton

collisions and solitons rotating around a central potential with both repulsive and attractive self-interactions. Conclusions and future directions are discussed in Section VI.

II. ULA EQUATIONS OF MOTION

Most dark matter models that assume ULAs do not include self-interaction terms. Constraints from observations require a very small ULA self-interaction strength. According to [34], constraints from the Bullet Cluster require that the repulsive coupling be

$$\lambda < 10^{-11} \left(\frac{m}{\text{eV}/c^2} \right)^{3/2}. \quad (3)$$

ULA dark matter in the high occupancy regime – e.g., Bose-Einstein condensate-like solitons – are normally described by the Schrödinger-Poisson equations [17, 35–49]. When self-interactions are included, the Schrödinger-Poisson equations become the non-linear Schrödinger-Poisson or Gross-Pitaevskii-Poisson equations (GPP) [1, 50]. Assuming a classical field with minimal coupling to gravity, the action takes the form:

$$S = \int d^4x \sqrt{-g} \left[g^{\mu\nu} \partial_\mu \phi \partial_\nu \phi - \frac{1}{2} m^2 \phi^2 - \lambda \phi^4 \right]. \quad (4)$$

Here, ϕ is the scalar field, m is the mass of the scalar field, and λ is the self-interaction strength. Finding the equations of motion in the Newtonian gauge, and writing the real scalar field ϕ in terms of a complex field ψ by

$$\phi = \frac{\hbar}{\sqrt{2m}} \left(\psi e^{-imt/\hbar} + \psi^* e^{imt/\hbar} \right) \quad (5)$$

(see [51]), we arrive at the GPP equations:

$$i\hbar\dot{\psi} = -\frac{\hbar^2}{2m} \nabla^2 \psi + m\Phi\psi + \frac{4\pi\hbar^2 a_s}{m} |\psi|^2 \psi \quad (6)$$

and

$$\nabla^2 \Phi = 4\pi G m |\psi|^2. \quad (7)$$

where a_s is the scattering length, ψ is the boson field, and Φ is the gravitational potential. The scattering length can be thought of as a measure of the self-coupling. When a_s is positive, the interaction is repulsive. When a_s is negative, the interaction is attractive [52]. In [1], the self-coupling is described using the dimensionless parameter λ . λ is given by

$$\lambda = \frac{8\pi a_s m c}{\hbar} = \frac{8\pi M_p^2 G m a_s}{\hbar^2} \quad (8)$$

where M_p is the Planck mass. Using the process found in [33], the non-dimensional form of the GPP equations are:

$$i\dot{\psi} = -\frac{1}{2} \nabla^2 \psi + \Phi\psi + \kappa |\psi|^2 \psi \quad (9)$$

and

$$\nabla^2\Phi = 4\pi|\psi|^2. \quad (10)$$

In this version of the GPP equations, κ is the dimensionless coupling constant. In going from Eq. 6 to Eq. 9, we find that

$$\kappa = \frac{4\pi\hbar a_s}{\mathcal{T}m^2G}, \quad (11)$$

where \mathcal{T} is the time scale given in [33]. It is also defined in the next section.

III. IMPLEMENTATION IN PYSIULTRALIGHT

PYULTRALIGHT is a Python solver for the evolution of solitonic dark matter and solves the Schrödinger-Poisson system of equations. The code uses a pseudospectral solver where the linear differential operators are computed in Fourier space whereas the non-linear terms are computed in phase space. We made the following changes to the code to adapt it for a self-coupling term, creating a version we refer to as PYSIULTRALIGHT.

Following a similar procedure as in [33], we re-derived the evolution equations in the presence of self interactions. First, we determined how ψ changes when a small step in time is taken:

$$\begin{aligned} \psi(\vec{x}, t+h) = T \exp \left[-i \int_t^{t+h} dt' \left(-\frac{1}{2}\nabla^2 + \Phi(\vec{x}, t') \right. \right. \\ \left. \left. + \kappa |\psi(\vec{x}, t')|^2 \right) \right] \psi(\vec{x}, t). \quad (12) \end{aligned}$$

Here, T is the time ordering operator. Next we use the following approximations for small time steps which come from the trapezoid rule.

$$\int_t^{t+h} dt' \Phi(\vec{x}, t') \approx \frac{h}{2} (\Phi(\vec{x}, t+h) + \Phi(\vec{x}, t)) \quad (13)$$

$$\int_t^{t+h} dt' \kappa |\psi(\vec{x}, t')|^2 \approx \frac{\kappa h}{2} (|\psi(\vec{x}, t+h)|^2 + |\psi(\vec{x}, t)|^2) \quad (14)$$

Substituting these into equation 12 gives:

$$\begin{aligned} \psi(\vec{x}, t+h) \approx \exp \left[-\frac{ih}{2}\Phi(\vec{x}, t+h) \right] \\ \exp \left[-\frac{ih\kappa}{2} |\psi(\vec{x}, t+h)|^2 \right] \\ \exp \left[-\frac{ih}{2}\nabla^2 \right] \exp \left[-\frac{ih}{2}\Phi(\vec{x}, t) \right] \\ \exp \left[-\frac{ih\kappa}{2} |\psi(\vec{x}, t)|^2 \right] \psi(\vec{x}, t). \quad (15) \end{aligned}$$

Using the Baker-Campbell-Hausdorff formula we verified that the error is $\mathcal{O}(\hbar^3)$. This is the same order of error as when there were no self interactions (i.e. when $\kappa = 0$). The procedure to evolve the soliton uses the following equations:

$$\begin{aligned} \psi(\vec{x}, t+h) = \exp \left[-\frac{ih}{2}\Phi(\vec{x}, t+h) \right] \\ \exp \left[-\frac{ih\kappa}{2} |\psi(\vec{x}, t+h)|^2 \right] \\ \mathcal{F}^{-1} \exp \left[-\frac{ih}{2}k^2 \right] \mathcal{F} \exp \left[-\frac{ih}{2}\Phi(\vec{x}, t) \right] \\ \exp \left[-\frac{ih\kappa}{2} |\psi(\vec{x}, t)|^2 \right] \psi(\vec{x}, t) \quad (16) \end{aligned}$$

$$\Phi(\vec{x}, t+h) = \mathcal{F}^{-1} \left(-\frac{1}{k^2} \right) \mathcal{F} 4\pi |\psi(\vec{x}, t_i)|^2. \quad (17)$$

Here, \mathcal{F} is the Fourier transform, \mathcal{F}^{-1} is the inverse Fourier transform, and k is the wavenumber in Fourier space. $\psi(\vec{x}, t_i)$ is the field at the half-step. We checked energy conservation to verify the integrity of changes we made to the code. The Lagrangian density that yielded the GPP equations is:

$$\mathcal{L} = - \left(\frac{1}{2} |\nabla\Phi|^2 + \Phi|\psi|^2 + \frac{1}{2} |\nabla\psi|^2 + \frac{i}{2} (\psi\dot{\psi}^* - \dot{\psi}\psi^*) + \frac{\kappa}{2} |\psi|^4 \right). \quad (18)$$

The energy of the system then becomes:

$$E_{tot} = \int_V d^3x \left(\frac{1}{2}\Phi|\psi|^2 - \frac{1}{2}\psi^*\nabla^2\psi + \frac{\kappa}{2}|\psi|^4 \right). \quad (19)$$

PYSIULTRALIGHT follows PYULTRALIGHT in using the following adimensional units. We will often refer to these units, which take the following form, as code units:

$$\mathcal{L} = \left(\frac{8\pi\hbar^2}{3m^2H_0^2\Omega_{m0}} \right)^{\frac{1}{4}} \approx 121 \left(\frac{10^{-23}\text{eV}}{m} \right)^{\frac{1}{2}} \text{ kpc}, \quad (20)$$

$$\mathcal{T} = \left(\frac{8\pi}{3H_0^2\Omega_{m0}} \right)^{\frac{1}{2}} \approx 75.5\text{Gyr}, \quad (21)$$

and

$$\begin{aligned} \mathcal{M} = \frac{1}{G} \left(\frac{8\pi}{3H_0^2\Omega_{m0}} \right)^{-\frac{1}{4}} \left(\frac{\hbar}{m} \right)^{\frac{3}{2}} \\ \approx 7 \times 10^7 \left(\frac{10^{-23}\text{eV}}{m} \right)^{\frac{3}{2}} M_{\odot}. \quad (22) \end{aligned}$$

These are the adimensional length, time, and mass respectively where H_0 is the present-day Hubble parameter and Ω_{m0} is the present-day matter fraction of the energy density of the universe. One can get dimensionful quantities back by using dimensional analysis. By taking a code unit and multiplying it by the proper adimensional quantities, one can recover the desired unit. For example, to recover the dimensional form of the energy:

$$E = \mathcal{M}\mathcal{L}^2\mathcal{T}^{-2}E_{code}. \quad (23)$$

To initialize the code, users must specify the initial soliton profiles by giving the solitons the desired masses, positions, velocities, and phases. In PYSIULTRALIGHT, the user must additionally specify the boson mass and the dimensionless coupling constant. Other parameters that must be specified are the box size (which is the size of the simulation), the duration of the simulation, the time step, and the interaction strength. The time step used in the code is independent of the self-interaction strength. It is only dependent on the resolution but may also be adjusted with the step factor.

PYSIULTRALIGHT uses periodic boundary conditions from PYULTRALIGHT which may have affected the results of this paper. Using periodic boundary conditions means that the space in which the simulation runs is topologically equivalent to a torus. When mass travels through the boundary, unphysical affects can arise because angular momentum is not conserved. There may also be unwanted effects when the box size is too small relative to the radius of the soliton. When this happens, the soliton may interact with its neighboring images in an unphysical way.

IV. SINGLE SOLITON BEHAVIOR IN PYSIULTRALIGHT

There are noticeable differences between simulations with large attractive self-interactions and those without self-interactions, indicating that it can be physically important to account for the presence of self-interactions. The first step to verify the newly adjusted program was working properly was to compare PYSIULTRALIGHT with zero self-coupling to PYULTRALIGHT. For the scenarios tested, there were no differences between the new and old versions. The next step in verifying the code was to ensure the energy of the system was conserved. We found that energy was indeed conserved, provided that the time step was sufficiently small.

We considered [1] as a benchmark for testing, and our next step was to show that PYSIULTRALIGHT outputs results which match those found there. In [1, 53, 54], axion dark matter with an attractive self-coupling has a maximum halo mass before the dark matter collapses into a black hole

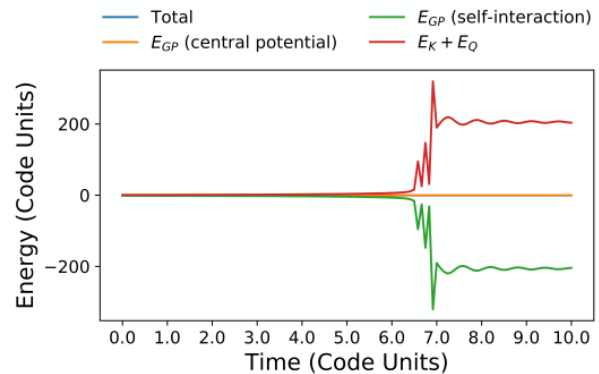


FIG. 1: The energy components (the total energy, the energy associated with a central potential, the gravitational potential energy, and the kinetic and quantum energies) of the collapsing soliton system. The total energy (in blue) is under the orange line.

$$M_{\max} = 1.012 \frac{\hbar}{\sqrt{Gm|a_s|}}, \quad (24)$$

which can be rewritten as,

$$\frac{M_{\max}}{M_{\odot}} = 1.56 \times 10^{-34} \left(\frac{\text{eV}/c^2}{m} \right)^{\frac{1}{2}} \left(\frac{\text{fm}}{|a_s|} \right)^{\frac{1}{2}}. \quad (25)$$

This means there are no time-independent solutions to the GPP equations when the soliton mass is too large and the self-interaction is attractive.

We first set up a scenario involving a single soliton with an attractive self-interaction and varied the mass of the soliton. Using $\kappa = -2.0$ and an axion mass of $m = 1 \times 10^{-22} \text{eV}/c^2$ (which corresponds to $a_s = -7.6 \times 10^{-60} \text{fm}$), the maximum mass of a soliton from Equation 25 is $M_{\max} = 5.66 \times 10^6 M_{\odot}$ or 2.46 code units. The starting simulation had the soliton mass at 2.5 code units which is larger than M_{\max} . We found that the soliton collapsed into a singularity which we define as when at least 0.25% of the total mass is contained in one unit cell. PYSIULTRALIGHT can only handle a grid-point to grid-point phase difference of up to $\pi/2$ which limits how dense the collapsed soliton can get. Fig 1 also shows the components of the system's energy over time. From this, we see that the total system energy is conserved up until the end of the collapse. For most of the simulation, energy is conserved to better than one part in 10^3 . After the soliton has collapsed, the total energy change is about 7 percent. This simulation was done with a step factor of 0.05 which is a measure of the temporal resolution. We found that decreasing the step factor greatly reduced the percent energy change when there are collapsing solitons.

In the first simulation testing the conditions for when to observe a collapsing soliton, the soliton had a mass of

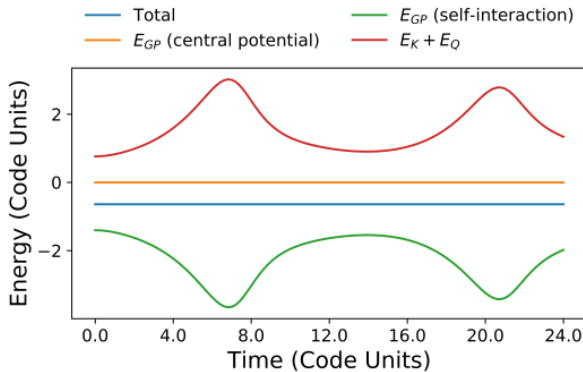


FIG. 2: Similar to Fig. 1: the energy components of an oscillating soliton system. Note that the total energy is conserved (to within 1 part in 10^4).

2.4 code units which is less than M_{\max} . In this situation, the soliton oscillated in size. In Fig. 2, we again see that energy is conserved to one part in 10^4 for a step factor of 1. For other simulations where the mass was less than M_{\max} , the solitons also oscillated. Similarly, for other simulations where the mass was greater than M_{\max} , the soliton collapsed. These results were consistent with results that appear in [1].

PYSiULTRALIGHT improves on its predecessor by adding the ability for the user to specify the radius of the soliton when there are attractive self-interactions. We used a Gaussian ansatz which is an approximate solution to the Gross-Pitaevskii-Poisson equations [1]. The form for the soliton using the Gaussian ansatz is

$$\psi(r, t) = \left[\frac{M}{\pi^{3/2} R(t)^3} \right]^{1/2} e^{-\frac{r^2}{2R(t)^2}} e^{imH(t)r^2/2\hbar} \quad (26)$$

where $R(t)$ is the a measure of the size of the soliton, r is the distance from the center of the soliton, and $H(t) = \frac{\dot{R}}{R}$. This should not be confused with the Hubble parameter. The dependence on the self-interaction is included in $H(t)$. There are other profiles we could have used [55], however, we wanted to compare our results with the claims in [1] which used a Gaussian ansatz. This profile is evolved using the GPP equations using the methods explained in Section III. PYULTRALIGHT makes a soliton profile by imposing spherical symmetry on the Schrödinger-Poisson equations and also requires that the radial density profile be time independent [33].

Using the Gaussian ansatz, we can test how solitons will oscillate given a specified mass and radius. There are two different scenarios where one can see oscillating solitons. The first scenario is when the soliton mass is below a critical mass $M_c = \frac{\sqrt{3}}{2} M_{\max}$. When this is the case, the soliton oscillates provided the starting radius is

larger than

$$R = \frac{1 + \sqrt{1 - \left(\frac{M}{M_c}\right)^2}}{2M}. \quad (27)$$

In the other scenario, the soliton mass is between the critical mass and the maximum mass. In this case, there is a finite range that the initial radius can be, otherwise the soliton will collapse. For oscillating solitons, there is a relation between the oscillation frequency and the equilibrium radius when oscillations are small. According to [1], the relation is given by

$$\omega^2 = \frac{2(R_e^2 - 1)}{R_e^4(R_e^2 + 1)}. \quad (28)$$

Here, R_e is equilibrium radius in terms of the radius of the soliton with a mass of M_{\max} and the frequency ω had been scaled by the dynamical time. The equilibrium radius is the radius where the effective potential as a function of radius is minimized. The equilibrium radius is given by

$$R_e = \frac{1 \pm \sqrt{1 - M^2}}{M}, \quad (29)$$

where M is the total soliton mass [1]. The dynamical time is given by

$$t_D = 3\sqrt{2} \frac{|a_s| \hbar}{Gm^2}. \quad (30)$$

We ran several simulations to determine the frequency of oscillations by analyzing the time for the soliton to go from a peak density to the next peak density. We do this because the density peak will occur when the soliton is smallest in size. For these simulations, the only parameter varied was the total soliton mass so as to isolate the relationship between the mass and the frequency of oscillation. The boson mass was $m = 1 \times 10^{-22} \text{eV}/c^2$, and the coupling was $\kappa = -2.0$. Fig. 3 shows the plot of the soliton equilibrium radius versus the oscillation frequency. The line in the plot shows the best fit of Eqn. 28 which fits the data well. The data does not match the best fit line as well when the mass approaches the maximum soliton mass.

The soliton oscillation frequency can also be found using total mass. Fig. 4 shows the soliton mass versus the oscillation frequency. For positive ω^2 , the equation is given by

$$\omega^2 = \frac{2M^4 \left(\sqrt{1 - M^2} - M^2 + 1 \right)}{\left(\sqrt{1 - M^2} + 1 \right)^5}. \quad (31)$$

Here, M is the soliton's mass in terms of the maximum soliton mass defined in Equation 24. The best fit dynamical time for both graphs was 0.786. This is longer than the calculated dynamical time of 0.675 code units.

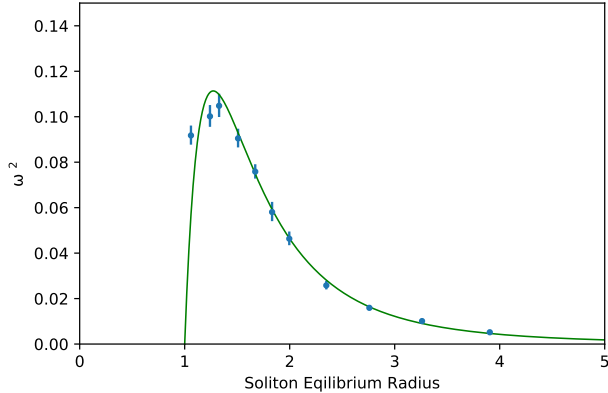


FIG. 3: This plot shows how changing the equilibrium radius changes the frequency of oscillation. The green line shows the fit of Equation 28 scaled by the best fit dynamical time squared.

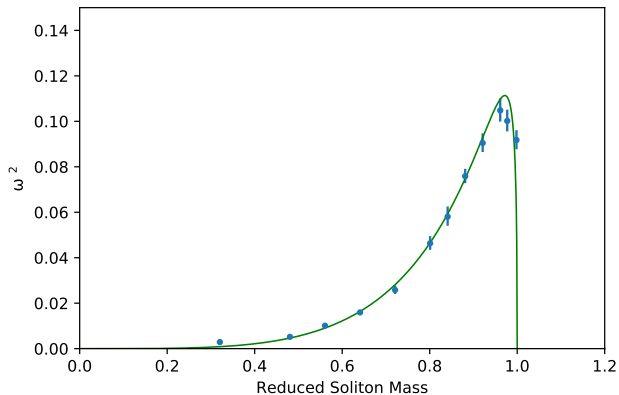


FIG. 4: This plot shows the changing the equilibrium radius changes the frequency of oscillation. The green line shows the fit of Equation 31 scaled by the best fit dynamical time squared.

The difference in these values is unlikely to be caused by a lack of spatial resolution because there was a negligible difference between the oscillation frequencies when the resolution was 256 versus 512. Another explanation is that the Gaussian profile deforms over time to a more realistic profile. We know this occurs because we fit a Gaussian to the density profile and looked at how the R-squared value changes over time. The value started at exactly 1 and evolved to approximately 0.998. This was also the value that the exact solution took. Since we know that the change in the profile has an effect on the maximum mass a soliton can have before collapsing [1, 55], it is reasonable to think that the oscillation frequencies might be scaled differently for the different profiles. We verified that this is the likely explanation by analytically calculating the dynamical time for the ex-

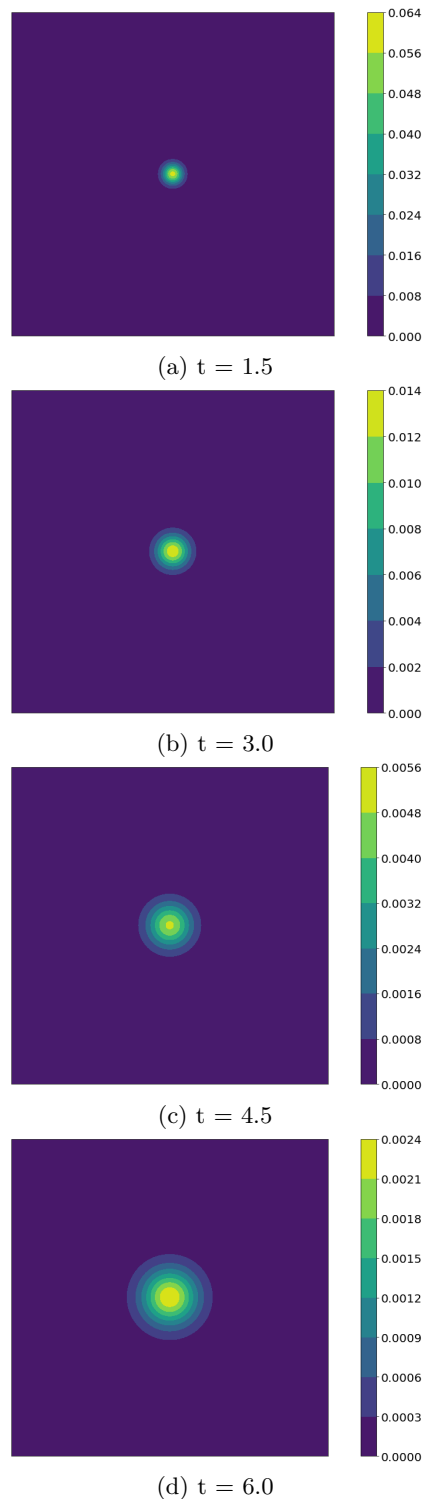


FIG. 5: A single soliton with a mass of 1.0 code units ($2.3 \times 10^6 M_\odot$) explodes. These plots show contours of constant density. Time progresses from top to bottom, and the time under each frame is indicated in code units. In the Gaussian ansatz, $R(0) = 1$ code unit. This is well below the critical mass of about 2.3 ($5.3 \times 10^6 M_\odot$) code units. Here, $\kappa = -2.0$. The box length is 45 code units and the time step is 0.3.

act solution and found that the dynamical time would be 0.791 code units. This new value matches well with the dynamical time found through the simulations.

According to [1], under certain initial conditions, we expect to see exploding solitons which are solitons that grow without bound. Specifically, when the soliton mass is below the critical mass $M_c = \frac{\sqrt{3}}{2} M_{\max}$ and the radius of the soliton is less than $R = \frac{1 + \sqrt{1 - (\frac{M}{M_c})^2}}{2M}$ but greater than the radius that maximizes the effective potential, explosions should occur. This value of the radius of the number of equilibrium radii of a soliton with mass M_{\max} (i.e. $R \equiv R_{eq}(M_{\max})$). Because the Gaussian ansatz is only an approximate solution, the criteria for observing different phenomena, such as collapsing solitons and oscillating solitons, changes slightly. For instance, the maximum mass for a soliton with a Gaussian form is $M_{\max} = 1.085 \frac{\hbar}{\sqrt{Gm|a_s|}}$ instead of the exact value of $M_{\max} = 1.012 \frac{\hbar}{\sqrt{Gm|a_s|}}$ [1].

In Fig. 5, we simulate a soliton with attractive self-interactions. The initial size is smaller than the critical radius. The mass is also below the critical mass. The soliton expands in size without collapsing again or oscillating in size. We find that with a sufficiently small radius, provided that the mass is less than a critical mass, the soliton collapses.

V. MULTIPLE SOLITON BEHAVIOR AND CENTRAL POTENTIAL EXAMPLES IN PYULTRALIGHT

PySiUltralight is capable of simulating multiple solitons simultaneously. In Fig. 6 through Fig. 9, two solitons move towards each other. The set-up differed only by a phase shift between solitons and the value of the self-coupling. In all the figures, the initial set up has two solitons, each of 20 code mass units ($4.6 \times 10^7 M_{\odot}$), spaced 1.2 code units (45.6kpc) apart moving towards each other with a relative velocity of 20 code units (9.8km/s). The duration in all the simulations is 0.1 code units which is about 7.6 Gyr. We chose this duration so that we would be able to compare our simulation results with those in [33]. In the scenarios where there is an attractive self-interaction, $\kappa = -0.02$ corresponding to $\lambda = -7.60 \times 10^{-62}$. When there are repulsive self-interactions, $\kappa = 0.02$. This corresponds to $\lambda = 7.60 \times 10^{-62}$. In these figures, the color scales are different in each frame in the same way that the scales are different in Fig. 5. These figures are useful schematically in understanding the behavior of these collisions. In Fig. 6, Fig. 7, and Fig. 10, there is no phase shift between solitons. The difference between these figures is that in Fig. 6, the solitons enter and leave the collision area unaltered while in Fig. 7 they are distorted. The solitons pass through each other unaffected which is to be expected when there is no self-interaction term. How-

ever, when there is an attractive self-interaction term, the solitons merge and then oscillate in size. There are only minor differences between Fig. 6 and Fig. 10. The biggest difference is that with the repulsive self-interaction, the resultant solitons are slightly larger in size. In Fig. 8, Fig. 9, and Fig. 11 there is a phase shift of π between the two solitons. This phase shift creates an effective repulsive force between the solitons [56]. As with the first three simulations, the main difference is how the solitons enter and exit the collision zone.

In [33], the authors run a simulation in PYULTRALIGHT where a soliton rotates around a central potential. We recreated this and then included an attractive self-interaction to see what differences exist with this inclusion of a self-coupling. For the set-up, an axion mass of $m = 1 \times 10^{-22} \text{eV}/c^2$ was used, the box length was 10 code units (380kpc), the duration was 0.4 code units (30.2Gyr), the central mass was 1000 code units ($2.3 \times 10^9 M_{\odot}$), the soliton mass was 12 code units ($2.8 \times 10^7 M_{\odot}$), the starting distance away from the central mass was 3 code units (114kpc), and the initial tangential velocity was 16 code units (7.9km/s). Fig. 12 shows three scenarios of a soliton orbiting around a central potential, one without self-interactions, one with an attractive self-interaction, and one with repulsive self-interactions. In this figure the colored lines represent constant density contours. As the soliton rotates around the central mass, the soliton stretches as the parts of the soliton closer to the center rotate faster than the outside portions. When we include an attractive self-interaction, we can see the the soliton is less disrupted than the case when there were no self-interactions. Simulations with repulsive self-interactions had the opposite effect in that the solitons became more spread out. Its important to note the colors of the solitons at different times do not necessarily correspond to the same density since the plots were overlaid.

VI. CONCLUSIONS

In this paper, we provide an outline for altering PYULTRALIGHT to include self-interactions. We provided background information on the physics of ultra-light dark matter and detailed the changes we made to PYULTRALIGHT. We tested the altered program's integrity by comparing the new version with the original version and by confirming energy was still conserved in the simulations. Using this altered version, we attempted to verify predictions made in [1] which quantified phenomena that one expects to see when ultra-light dark matter has attractive self-interactions. The predictions for finding a maximum mass for a soliton with attractive self-interactions matched well. The oscillation frequency predictions behaved similarly to predictions but had a different dynamical time. This discrepancy is likely caused by the approximate solution of the Gaussian profile being adjusted as the simulation progressed. We looked at

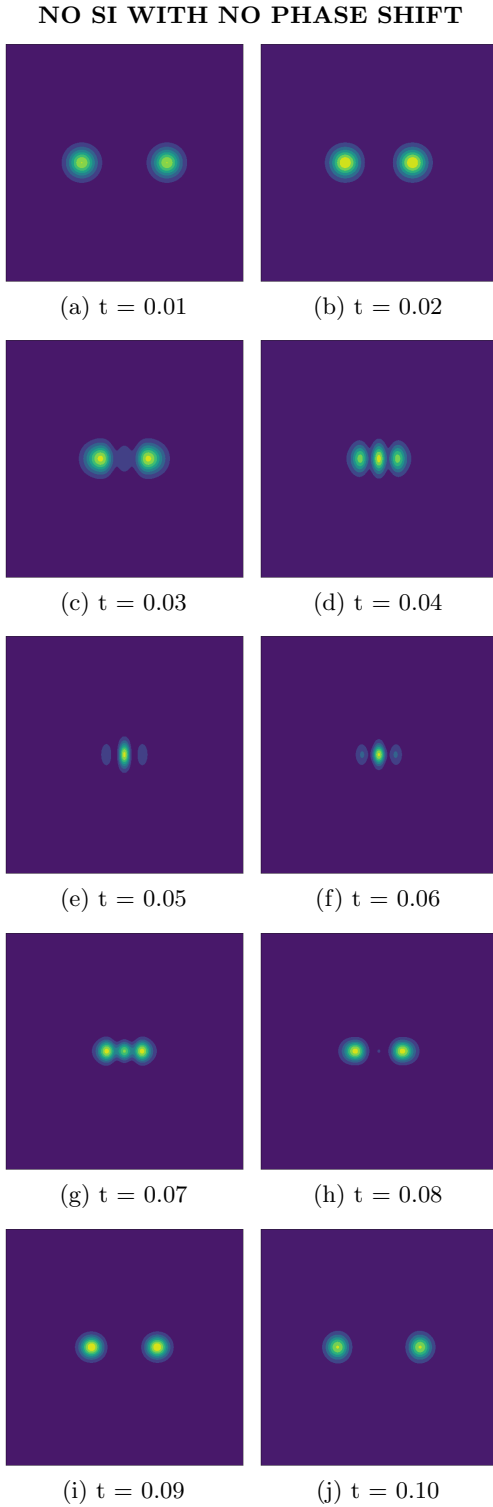


FIG. 6: Two colliding solitons with no phase shift and no self-interaction. These plots show contours of constant density. Time progresses across each row left to right, and the time under each frame is indicated in code units. The total duration of the simulation is 7.6 Gyr. The two solitons have the same shape and size from when they leave the collision area and when they enter. Each soliton passes through the other unaffected.

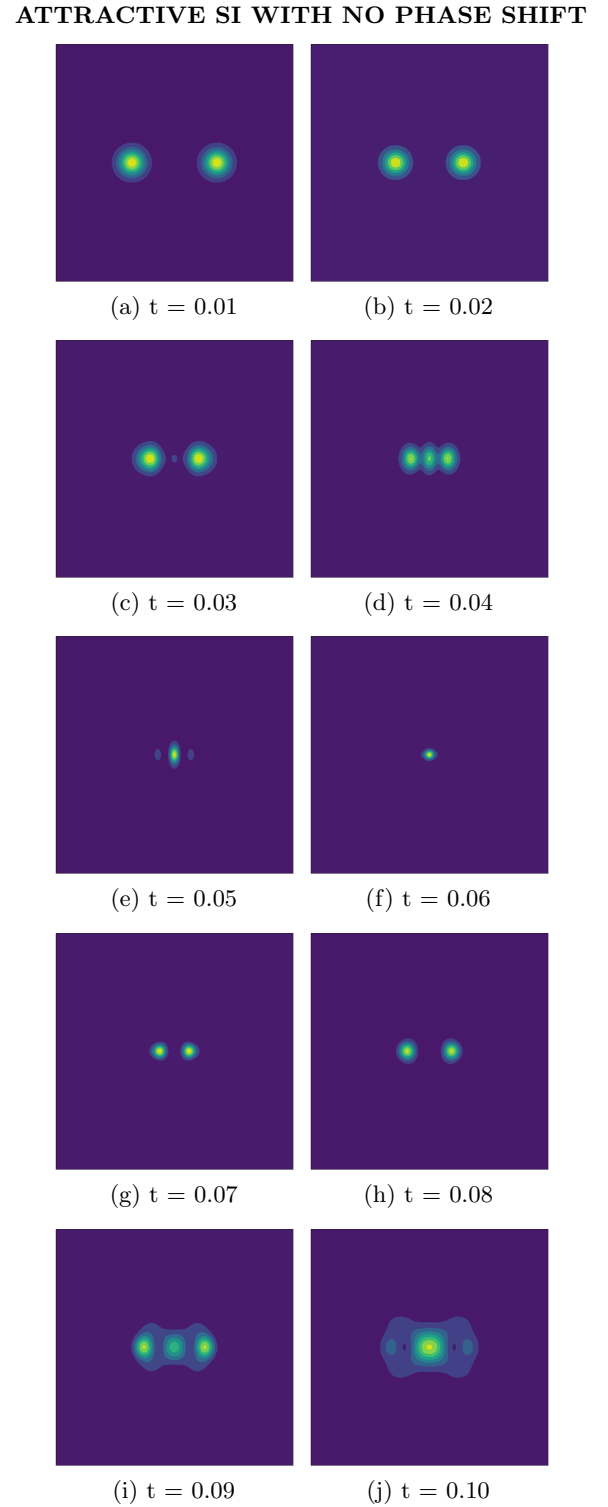


FIG. 7: Two colliding solitons with no phase shift with an attractive self-interaction. These plots show contours of constant density. Time progresses across each row left to right, and the time under each frame is indicated in code units. The duration for the simulation is 7.6 Gyr. $\kappa = -0.02$ or $\lambda = -7.60 \times 10^{-62}$. The inclusion of an attractive self interaction causes the solitons to become distorted. With relatively small masses, the solitons don't collapse into a black hole, and instead merge and oscillate in size.

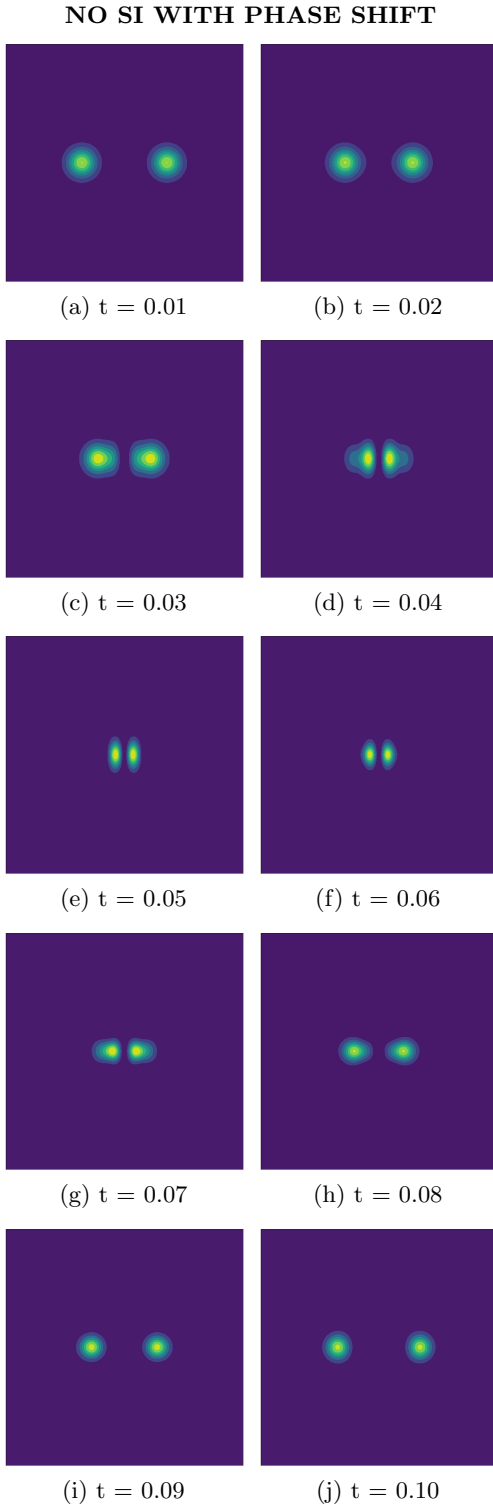


FIG. 8: Two colliding solitons with a phase shift of π and no self-interaction. These plots show contours of constant density. Time progresses across each row left to right, and the time under each frame is indicated in code units. The total duration of the simulation is 7.6 Gyr. The effective repulsive force from the phase difference causes the solitons to decelerate and then move in opposite directions. The initial and final soliton profiles are the same.

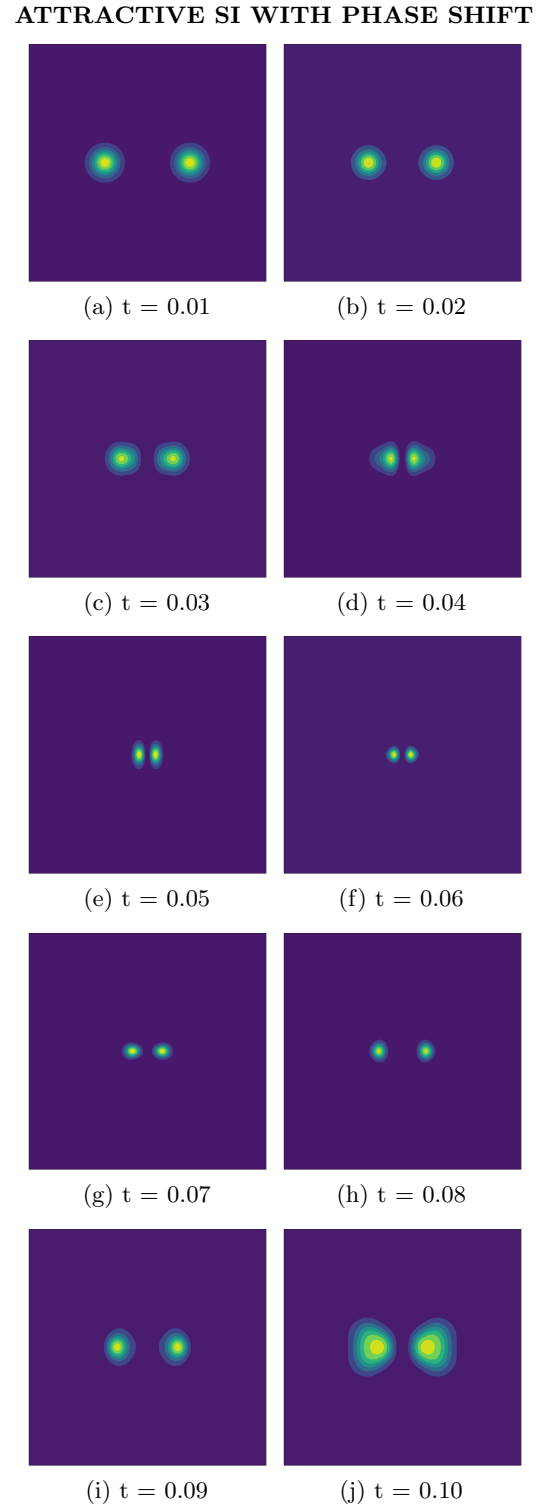


FIG. 9: Two colliding solitons with a phase shift of π with an attractive self-interaction. These plots show contours of constant density. Time progresses across each row left to right, and the time under each frame is indicated in code units. The total duration is 7.6 Gyr. $\kappa = -0.02$ or $\lambda = -7.60 \times 10^{-62}$. The repulsive force caused by the phase shift is strong enough to repel the solitons, however, the attractive self-interaction still causes the solitons to oscillate in size.

REPULSIVE SI WITH NO PHASE SHIFT

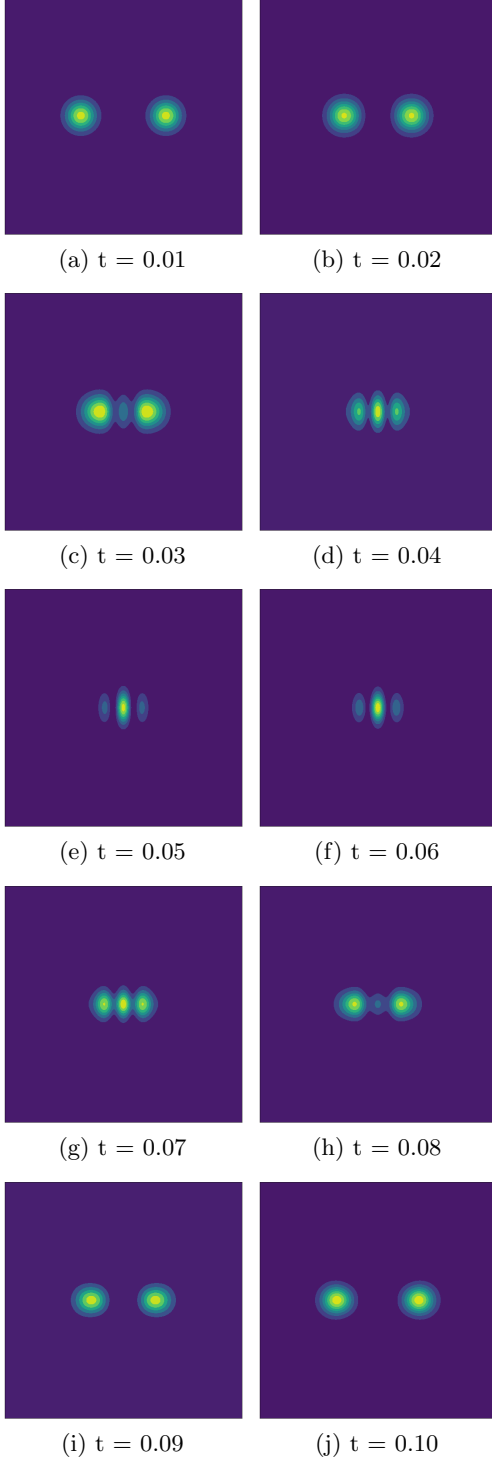


FIG. 10: Two colliding solitons with no phase shift with a repulsive self-interaction. These plots show contours of constant density. Time progresses across each row left to right, and the time under each frame is indicated in code units. The duration is 7.6 Gyr. $\kappa = 0.02$ or $\lambda = 7.60 \times 10^{-62}$. The results are similar to that in Fig. 6 but with the resultant solitons slightly enlarged. There are also minor differences in the intermediate time steps.

REPULSIVE SI WITH PHASE SHIFT

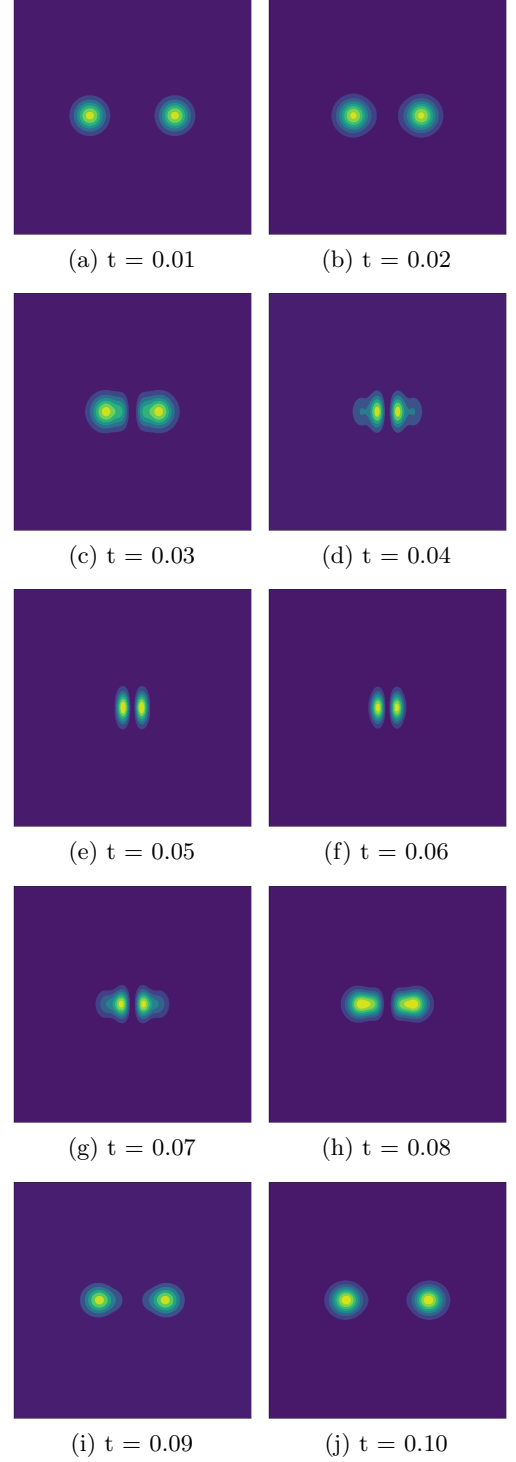


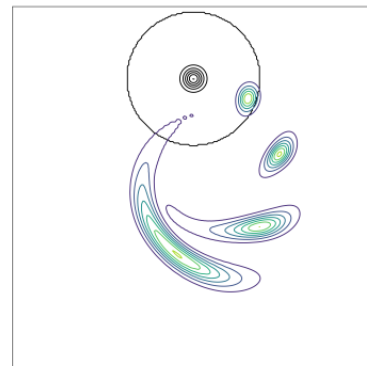
FIG. 11: Two colliding solitons with a phase shift of π with a repulsive self-interaction. These plots show contours of constant density. Time progresses across each row left to right, and the time under each frame is indicated in code units. The duration is 7.6 Gyr. $\kappa = 0.02$ or $\lambda = 7.60 \times 10^{-62}$. The results are similar to that in Fig. 8.

the conditions needed to see exploding solitons by using an approximate Gaussian soliton profile. When the soliton mass was less than the critical mass and the starting soliton size was sufficiently small, we saw the soliton explode.

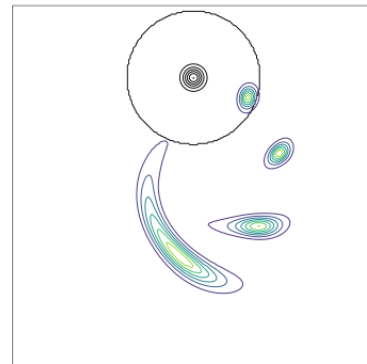
We also ran simulations that compared situations with attractive self-interactions, repulsive self-interactions, and without self-interactions, including binary soliton collisions and solitons rotating around a central potential. Qualitatively, there were noticeable differences when self-interactions were introduced in these scenarios. The attractive self-interactions cause the solitons to more easily stick to one another which is to be expected. Attractive self-interactions also made it more difficult for the solitons to be tidally disrupted when the solitons rotated around the central potential. We also found that having repulsive self-interactions had the effect of spreading out the soliton profile more when orbiting a central potential. For future work, we would like to implement other boundary conditions to see how they affect the simulation results. Other future goals include adding the ability to have multiple species of ALPs to the simulations and coupling terms between ALPs with different masses.

ACKNOWLEDGMENTS

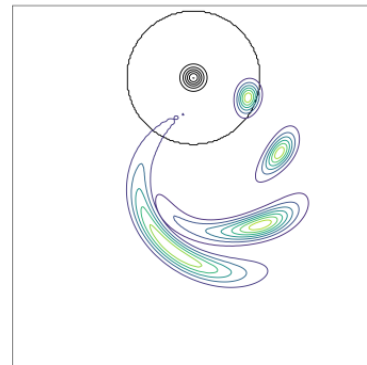
We would like to thank Lisa Bouchard, Annika Peter, Arka Banerjee, and Katelin Schutz for offering comments on this paper. We would like to thank Adam Dukehart for his insight on how the energy changes with the inclusion of self-interactions. We would also like to thank Ethan Nadler and J. Luna Zagorac for their helpful discussions about our simulations results. We thank Richard Easther, Brian Nord, Nathan Musoke, Anthony Mirasola, Kay Kirkpatrick, Ed Copeland, Risa Wechsler, and Juna Kollmeier for additional helpful conversations. CPW would like to thank all workers who made this research possible, especially those at the University of New Hampshire, the Aspen Center for Physics, which is supported by National Science Foundation (NSF) grant PHY-1607611, and the Kavli Institute for Theoretical Physics, where this research was supported in part by the NSF under Grant No. PHY-1748958. CPW's contributions to this project were also supported by DOE Grant DE-SC0020220. This paper honors the memory of Breonna Taylor.



(a) No self-interactions



(b) Attractive self-interactions



(c) Repulsive self-interactions

FIG. 12: Plot (a) shows how a soliton behaves when rotating around a central potential at different times when there are no self-interactions. Plot (b) has the same initial conditions except it has a coupling of $\kappa = -0.05$. The most noticeable difference between the two plots is that the soliton with an attractive self-interaction is less spread out by the central potential. Plot (c) has a repulsive coupling of $\kappa = 0.05$. Here, we see that the soliton is more spread out than the simulations with no coupling or with an attractive coupling.

- [1] P.-H. Chavanis, Phys. Rev. **D94**, 083007 (2016), arXiv:1604.05904 [astro-ph.CO].
- [2] M. R. Buckley and A. H. Peter, Physics Reports **761**, 1–60 (2018).
- [3] P. A. R. Ade *et al.* (Planck), Astron. Astrophys. **594**, A13 (2016), arXiv:1502.01589 [astro-ph.CO].
- [4] B. Schwabe, J. C. Niemeyer, and J. F. Engels, Phys. Rev. **D94**, 043513 (2016), arXiv:1606.05151 [astro-ph.CO].
- [5] C. Armendariz-Picon and J. T. Neelakanta, Journal of Cosmology and Astroparticle Physics **2014**, 049–049 (2014).
- [6] G. Giesen, J. Lesgourgues, B. Audren, and Y. Ali-Haïmoud, JCAP **1212**, 008 (2012), arXiv:1209.0247 [astro-ph.CO].
- [7] N. Aghanim, Y. Akrami, M. Ashdown, J. Aumont, C. Baccigalupi, M. Ballardini, A. J. Banday, R. B. Barreiro, N. Bartolo, and *et al.*, Astronomy & Astrophysics **641**, A6 (2020).
- [8] A. Del Popolo and F. Pace, Astrophysics and Space Science **361** (2016), 10.1007/s10509-016-2742-z.
- [9] D. Marsh, Physical Review D (2015).
- [10] D. N. Spergel and P. J. Steinhardt, Phys. Rev. Lett. **84**, 3760 (2000).
- [11] V. Avila-Reese, P. Colin, O. Valenzuela, E. D’Onghia, and C. Firmani, The Astrophysical Journal **559**, 516 (2001).
- [12] M. Kamionkowski and A. R. Liddle, Phys. Rev. Lett. **84**, 4525 (2000).
- [13] E. Papastergis, R. Giovanelli, M. P. Haynes, and F. Shankar, Astron. Astrophys. **574**, A113 (2015), arXiv:1407.4665 [astro-ph.GA].
- [14] A. Arvanitaki, S. Dimopoulos, S. Dubovsky, N. Kaloper, and J. March-Russell, Physical Review D **81** (2010), 10.1103/physrevd.81.123530.
- [15] M. Cicoli, “Axion-like particles from string compactifications,” (2013), arXiv:1309.6988 [hep-th].
- [16] R. D. Peccei and H. R. Quinn, Phys. Rev. Lett. **38**, 1440 (1977), [328(1977)].
- [17] A. H. Guth, M. P. Hertzberg, and C. Prescod-Weinstein, Physical Review D **92** (2015), 10.1103/physrevd.92.103513.
- [18] M. Dine and W. Fischler, Physics Letters **120B** (1983).
- [19] J. Preskill, M. Wise, and F. Wilczek, Physics Letters **120B** (1983).
- [20] L. F. Abbott and P. Sikivie, Physics Letters **120B** (1983).
- [21] J. E. Kim and G. Carosi, Rev. Mod. Phys. **82**, 557 (2010).
- [22] D. Alesini, C. Braggio, G. Carugno, N. Crescini, D. D’Agostino, D. Di Gioacchino, R. Di Vora, P. Falferi, S. Gallo, U. Gambardella, and *et al.*, Physical Review D **99** (2019), 10.1103/physrevd.99.101101.
- [23] W. Hu, R. Barkana, and A. Gruzinov, Physical Review Letters **85** (2000).
- [24] L. Hui, J. Ostriker, S. Tremaine, and E. Witten, Physical Review D **95** (2017).
- [25] A. Ringwald, Physics of the Dark Universe **1**, 116 (2012).
- [26] E. Madelung, Naturwissenschaften **14**, 1004 (1926).
- [27] H.-Y. Schive, T. Chiueh, and T. Broadhurst, Nature Physics **10**, 496–499 (2014).
- [28] H.-Y. Schive, M.-H. Liao, T.-P. Woo, S.-K. Wong, T. Chiueh, T. Broadhurst, and W.-Y. P. Hwang, Physical Review Letters **113** (2014), 10.1103/physrevlett.113.261302.
- [29] A. Suárez and P.-H. Chavanis, Physical Review D **98** (2018), 10.1103/physrevd.98.083529.
- [30] A. Vaquero, J. Redondo, and J. Stadler, JCAP **2019**, 012 (2019), arXiv:1809.09241 [astro-ph.CO].
- [31] B. J. Kavanagh, T. D. P. Edwards, L. Visinelli, and C. Weniger, “Stellar disruption of axion miniclusters in the milky way,” (2020), arXiv:2011.05377 [astro-ph.GA].
- [32] P. Chavanis, M. Lemou, and F. Méhats, Phys. Rev. D (2015).
- [33] F. Edwards, E. Kendall, S. Hotchkiss, and R. Easther, JCAP **1810**, 027 (2018), arXiv:1807.04037 [astro-ph.CO].
- [34] J. Fan, “Ultralight repulsive dark matter and bec,” (2016), arXiv:1603.06580 [hep-ph].
- [35] D. J. E. Marsh, Phys. Rept. **643**, 1 (2016), arXiv:1510.07633 [astro-ph.CO].
- [36] M. Baldeschi, G. Gelmini, and R. Ruffini, Physics Letters B **122** (1983).
- [37] S. Sin, Physical Review D **50** (1994).
- [38] J.-w. Lee and I.-g. Koh, Phys. Rev. D **53**, 2236 (1996).
- [39] T. Matos, F. S. Guzmán, and L. A. Ureña-López, Classical and Quantum Gravity **17** (2000).
- [40] P. J. E. Peebles, The Astrophysical Journal Letters **534** (2000).
- [41] J.-W. Lee, Phys. Lett. **B756**, 166 (2016), arXiv:1511.06611 [astro-ph.GA].
- [42] A. Arbey, J. Lesgourgues, and P. Salati, Phys. Rev. D **64**, 123528 (2001).
- [43] M. Alcubierre, F. S. Guzman, T. Matos, D. Nunez, L. A. Urena-Lopez, and P. Wiederhold, Class. Quant. Grav. **19**, 5017 (2002), arXiv:gr-qc/0110102 [gr-qc].
- [44] M. P. Silverman and R. L. Mallett, General Relativity and Gravitation **34** (2002).
- [45] A. Arbey, J. Lesgourgues, and P. Salati, Phys. Rev. D **68**, 023511 (2003).
- [46] C. G. Bohmer and T. Harko, Journal of Cosmology and Astroparticle Physics (2007).
- [47] T. Fukuyama, M. Morikawa, and T. Tatekawa, Journal of Cosmology and Astroparticle Physics **2008**, 033 (2008).
- [48] P. Sikivie and Q. Yang, Phys. Rev. Lett. **103**, 111301 (2009).
- [49] J.-W. Lee and S. Lim, Journal of Cosmology and Astroparticle Physics **2010**, 007 (2010).
- [50] P. H. Chavanis and L. Delfini, Phys. Rev. **D84**, 043532 (2011), arXiv:1103.2054 [astro-ph.CO].
- [51] K. Kirkpatrick, A. E. Mirasola, and C. Prescod-Weinstein, “Relaxation times for bose-einstein condensation in axion miniclusters,” (2020), arXiv:2007.07438 [hep-ph].
- [52] W. Bao and Y. Cai, Kinetic and Related Models **6**, arXiv:1212.5341 (2013), arXiv:1212.5341 [cond-mat.quant-gas].
- [53] J. Eby, M. Leembruggen, P. Suranyi, and L. C. R. Wijewardhana, Journal of High Energy Physics **2016** (2016), 10.1007/jhep12(2016)066.
- [54] J. Chen, X. Du, E. W. Lentz, D. J. E. Marsh, and J. C. Niemeyer, “New insights into the formation and growth of boson stars in dark matter halos,” (2020), arXiv:2011.01333 [astro-ph.CO].

- [55] J. Eby, M. Leembruggen, L. Street, P. Suranyi, and L. C. R. Wijewardhana, 10.1103/PhysRevD.98.123013.
- [56] A. Paredes and H. Michinel, Phys. Dark Univ. **12**, 50 (2016), arXiv:1512.05121 [astro-ph.CO].